GEOPHYSICS, VOL. 81, NO. 2 (MARCH-APRIL 2016); P. E113–E128, 13 FIGS., 8 TABLES.
10.1190/GEO2015-0174.1

Three effective inverse Laplace transform algorithms for computing time-domain electromagnetic responses

Jianhui Li[1], Colin G. Farquharson[2], and Xiangyun Hu[3]

ABSTRACT

The inverse Laplace transform is one of the methods used to obtain time-domain electromagnetic (EM) responses in geophysics. The Gaver-Stehfest algorithm has so far been the most popular technique to compute the Laplace transform in the context of transient electromagnetics. However, the accuracy of the Gaver-Stehfest algorithm, even when using double-precision arithmetic, is relatively low at late times due to round-off errors. To overcome this issue, we have applied variable-precision arithmetic in the MATLAB computing environment to an implementation of the Gaver-Stehfest algorithm. This approach has proved to be effective in terms of improving accuracy, but it is computationally expensive. In addition, the Gaver-Stehfest algorithm is significantly problem dependent. Therefore, we have turned our attention to two other algorithms for computing inverse Laplace transforms, namely, the Euler and Talbot algorithms. Using as examples the responses for central-loop, fixed-loop, and horizontal electric dipole sources for homogeneous and layered mediums, these two algorithms, implemented using normal double-precision arithmetic, have been shown to provide more accurate results and to be less problem dependent than the standard Gaver-Stehfest algorithm. Furthermore, they have the capacity for yielding more accurate time-domain responses than the cosine and sine transforms for which the frequency-domain responses are obtained by interpolation between a limited number of explicitly computed frequency-domain responses. In addition, the Euler and Talbot algorithms have the potential of requiring fewer Laplace- or frequency-domain function evaluations than do the other transform methods commonly used to compute time-domain EM responses, and thus of providing a more efficient option.

INTRODUCTION

The time-domain electromagnetic (EM) method plays an important role in a wide range of geophysical applications including mineral exploration (e.g., Flores and Peralta-Ortega, 2009; Yang and Oldenburg, 2012; Xue et al., 2014), hydrocarbon exploration (e.g., Constable, 2010; Swidinsky et al., 2013; Barsukov and Fainberg, 2014), and environmental or hydrogeological investigations (e.g., Meju et al., 2000; d'Ozouville et al., 2008; Porsani et al., 2012). Computing synthetic data for specific acquisition systems and configurations and for prospective earth models is essential for feasibility analysis, survey design, and data inversion and interpretation.

Synthesizing data for the time-domain method is typically more complex than for the frequency-domain case. For some simple models and particular configurations of sources and receivers, analytic methods do exist. For example, Goldman and Fitterman (1987) present a technique for computing the transient response excited by a rectangular loop on the surface of a two-layer medium directly in the time domain. For more general scenarios, however, the only possibilities are numerical solutions of the time-dependent partial differential equation. This can be performed by time stepping, or by the so-called spectral method in which the partial differential equation is transformed to the frequency or Laplace domain, solved numerically in this domain, and the time-domain responses obtained by inverse Fourier or Laplace transformation.

The most common algorithms used to compute the inverse Fourier transforms of EM geophysics are the cosine and sine transforms that use a digital filtering method (Anderson, 1983; Newman et al.,

Manuscript received by the Editor 13 March 2015; revised manuscript received 3 November 2015; published online 14 March 2016.
[1]China University of Geosciences, Institute of Geophysics and Geomatics, Wuhan, Hubei, China; Memorial University of Newfoundland, Department of Earth Sciences, St. John's, Newfoundland and Labrador, Canada; and China University of Mining & Technology, State Key Laboratory for GeoMechanics and Deep Underground Engineering, Xuzhou, Jiangsu, China. Email: ljhiiicumt@126.com.
[2]Memorial University of Newfoundland, Department of Earth Sciences, St. John's, Newfoundland and Labrador, Canada. E-mail: cgfarquh@mun.ca.
[3]China University of Geosciences, Institute of Geophysics and Geomatics, Wuhan, Hubei, China. E-mail: xyhu@cug.edu.cn.

1986). The fast Fourier transform (FFT) algorithm has also been used (Jang et al., 2013), although the number of frequencies required for the FFT algorithm is very large, and simple interpolation over sparsely sampled frequency-domain responses does not give accurate results (Hohmann, 1983; Newman et al., 1986). Typically, for the digital filter method, dozens of frequency-domain responses distributed evenly in terms of the logarithm of frequency over a broad spectral bandwidth are computed directly, and then cubic spline interpolation is used to obtain the few hundred frequency-domain response estimates needed for the filtering. The lagged convolution approach of Anderson (1983) enables the same frequency-domain responses to be reused in the calculation of the responses at multiple times. The digital filtering approach using cosine and sine transforms has been shown to provide good accuracy and efficiency in many geophysical contexts (e.g., Newman et al., 1986; Gupta et al., 1989; Key, 2012), and has been used successfully for modeling and inversion (e.g., Farquharson and Oldenburg, 1993; Effersø et al., 1999; Börner et al., 2008; Li and Constable, 2010; Connell and Key, 2013; Sasaki et al., 2015).

An alternative to the cosine and sine digital filtering technique is the Gaver-Stehfest algorithm (Stehfest, 1970; Knight and Raiche, 1982). The Gaver-Stehfest algorithm has its own particular strengths: ease of implementation and its use of only real numbers for the coefficients and the Laplace-domain variable (Swidinsky et al., 2013). However, it also has weaknesses. In the Gaver-Stehfest algorithm, the values of the Laplace-domain variable at which the Laplace-domain response must be sampled are inversely proportional to the time at which the time-domain response is desired. Hence, it is necessary to recompute the Laplace-domain EM response for every given time. The overall computation time, therefore, increases substantially as the number of observation times increases. In addition, the accuracy of the Gaver-Stehfest algorithm, when implemented using typical double-precision arithmetic, can be poor (Raiche, 1987; Effersø et al., 1999; Everett, 2009). In spite of these shortcomings, the Gaver-Stehfest algorithm has been widely used in computing time-domain EM responses (e.g., Knight and Raiche, 1982; Raiche et al., 1985; Flis et al., 1989; Everett and Edwards, 1993; Swidinsky and Edwards, 2009; Li et al., 2011; Swidinsky et al., 2013).

In addition to the Gaver-Stehfest algorithm, more than 100 algorithms exist for the numerical inversion of a Laplace transform. The most popular algorithms can be divided into four categories, namely, the Gaver functionals method, Fourier series method, Talbot algorithm, and Weeks algorithm (Abate and Valkó, 2004; Kuhlman, 2013). The first three categories can be expressed within a unified framework (Abate and Whitt, 2006). We will in turn give a brief introduction for each of these four categories. First, the Gaver functionals method refers to use of an acceleration scheme to speed up the convergence of the Gaver functionals sequence, which is a direct approximation of the inverse Laplace transform integral. There are several acceleration schemes, for example, Saltzer summation proposed by Stehfest (and known as the Gaver-Stehfest algorithm) and Wynn's rho algorithm (known as Gaver-Wynn's rho algorithm; Valkó and Abate, 2004). Second, for the Fourier series method, the original expression of the inverse Laplace transform is converted into a Fourier transform, evaluation of which usually needs an approach to accelerate convergence, such as the Padé approximation or expansions with Euler summation (Kuhlman, 2013). The latter approach, which is known as the Euler algorithm, uses Euler summation to accelerate the convergence of an infinite Fourier series that is used to approximate the original inversion integral (Abate and Whitt, 1992; Abate et al., 1999). Third, the Talbot algorithm applies a deformed Bromwich contour in the complex plane to the original integral of the inverse Laplace transform (Talbot, 1979). This algorithm has some improved versions, for example, the fixed-Talbot algorithm (Abate and Valkó, 2004). Finally, the Weeks algorithm returns an explicit expression for the time-domain function to be solved as an expansion in weighted Laguerre polynomials, the coefficients of which are computed based on the Bromwich integration in the complex plane (Weeks, 1966; Abate et al., 1996). Unlike for the other inverse Laplace transform algorithms, the Laplace-domain variable for the Weeks method is independent of the observation time. It is, therefore, appropriate to use for many observation times (Kano et al., 2005; Kuhlman, 2013). However, the Weeks algorithm has two problem-dependent parameters, for the determination and tuning of which there is no effective method.

In this paper, our motivation is the identification of improved computational approaches for calculating inverse Laplace transforms relevant to EM geophysics. Two particular issues are considered: (1) improving upon the accuracy of the Gaver-Stehfest algorithm using variable-precision arithmetic and (2) investigating the performance of the Euler and Talbot algorithms, and presenting these two algorithms as alternatives to the Gaver-Stehfest algorithm, and to digital filtering methods, for computing time-domain EM responses.

METHODS

In this section, we give the final expressions for the Gaver-Stehfest, Euler, and Talbot algorithms. For more information about these algorithms, including derivations, please see Abate and Whitt (2006). Suppose a function $\hat{f}(s)$ is available in the Laplace domain, and the corresponding function $f(t)$ is required in the time domain.

Gaver-Stehfest algorithm

The Gaver-Stehfest approximation $f_G(t)$ to $f(t)$ is defined by (Everett, 2009)

$$f_G(t) = \frac{\ln 2}{t} \sum_{m=1}^{M} c_m^G \hat{f}\left(\frac{m \ln 2}{t}\right), \tag{1}$$

where M is an even positive integer that denotes the number of terms included in the summation and hence the number of Gaver-Stehfest coefficients required. The discrete form of the Laplace-domain variable is $s = m \ln 2/t$. The coefficients c_m^G are computed by

$$c_m^G = (-1)^{\frac{M}{2}+m} \sum_{k=\lfloor \frac{m+1}{2} \rfloor}^{\min\{m,\frac{M}{2}\}} \frac{k^{M/2}(2k)!}{\left(\frac{M}{2}-k\right)!k!(k-1)!(m-k)!(2k-m)!}, \tag{2}$$

where $[m + 1/2]$ stands for the greatest integer less than or equal to $m + 1/2$. As shown in equation 2, the coefficient c_m^G includes multiple binomial coefficients, which become large as m increases. Therefore, computation of the coefficients c_m^G is numerically unsta-

ble for large M in a fixed-precision computing environment due to the propagation of round-off errors (Montella et al., 2007). In addition, c_m^G has an alternating sign, which causes cancellation issues. Table 1 summarizes the required precision and number of accurate digits, among other information, for the methods considered here as estimated by Abate and Whitt (2006). As this table shows, the system precision required (i.e., the available decimal digits) is $1.1M$ for the Gaver-Stehfest algorithm. For example, in a computing environment of 15 decimal digits, once M is larger than 14, for which the value of 1.1×14 is equal to 15.4 and is thus greater than the number of decimal digits, the numerical calculations for c_m^G must be expected to be polluted by round-off errors.

Euler algorithm

The Euler algorithm is one of the Fourier series methods of evaluating the inverse Laplace transform. Unlike the Gaver-Stehfest algorithm, the formulation of the Euler algorithm contains complex numbers. Its approximation $f_E(t)$ to $f(t)$ is as follows (Abate and Whitt, 2006):

$$f_E(t) = \frac{10^{M/3}}{t} \sum_{m=0}^{2M} c_m^E \, \mathrm{Re}\left(\hat{f}\left(\frac{\beta_m}{t}\right)\right). \tag{3}$$

In equation 3, β_m/t is the Laplace-domain discrete variable, where $\beta_m = M \ln(10)/3 + i\pi m$ and $i = \sqrt{-1}$. The coefficients c_m^E are defined as follows:

$$c_m^E = (-1)^m \xi_m, \tag{4}$$

where the range of m is from 0 to $2M$. The ξ_m is determined as follows: $\xi_0 = 0.5$, $\xi_m = 1$ for $1 \le m \le M$, $\xi_{2M} = 2^{-M}$, $\xi_{2M-m} = \xi_{2M-m+1} + 2^{-M} M!/(m!(M-m)!)$ for $0 < m < M$. As indicated in Table 1, the maximum M free of round-off errors for the Euler algorithm is 7 in a computing environment of 15 decimal digits, and the corresponding number of function evaluations required is 15. In spite of involving factorials, the coefficient formulas here are still simpler than those for the Gaver-Stehfest algorithm. Therefore, this algorithm suffers from round-off errors to a lesser extent than the Gaver-Stehfest algorithm.

Talbot algorithm

As a modification of the original Talbot algorithm, the fixed-Talbot algorithm is characterized by the number of coefficients (Abate and Valkó, 2004). For this algorithm, the approximation $f_T(t)$ to $f(t)$ is given by Abate and Whitt (2006) as follows:

$$f_T(t) = \frac{2}{5t} \sum_{m=0}^{M-1} \mathrm{Re}\left(c_m^T \hat{f}\left(\frac{\delta_m}{t}\right)\right). \tag{5}$$

Here, the Laplace-domain discrete variable is more complicated than for the other two algorithms above: It is $s = \delta_m/t$ where $\delta_0 = 2M/5$, $\delta_m = 2m\pi/5(\cot(m\pi/M) + i)$ for $0 < m < M$, where, as before, $i = \sqrt{-1}$. The coefficients are also complex numbers and are related to δ_m:

$$c_0^T = \frac{1}{2} e^{\delta_0}, \tag{6}$$

$$c_m^T = \left[1 + i\left(\frac{m\pi}{M}\right)\left(1 + \left[\cot\left(\frac{m\pi}{M}\right)\right]^2\right) - i\cot\left(\frac{m\pi}{M}\right)\right] e^{\delta_m} \tag{7}$$

for $0 < m < M$. In a computing environment of 15 decimal digits, the maximum M free of round-off errors for the Talbot algorithm is 15 (see Table 1). Unlike the previous two algorithms, the coefficients in equations 6 and 7 do not involve factorials. This means that the Talbot algorithm itself is not nearly as susceptible to round-off errors as are the previous two methods, and it is able to employ an M of larger than 15 even in an environment of 15 digits.

As already indicated, the theoretical performance of the above three methods as described by Abate and Whitt (2006) based on the idealized scenarios is summarized in Table 1. The Gaver-Stehfest algorithm has the greatest requirement of system precision in terms of obtaining a desired number of accurate decimal digits, and it gives the lowest number of correct significant digits for a particular value of M. Its efficiency, therefore, is lower than the other two methods, which have the same efficiency. In other words, the Euler and Talbot algorithms can yield more accurate solutions in fixed-precision computing environments.

Cosine and sine transforms

Cosine and sine transforms are considered to be accurate and efficient algorithms for computing transient EM responses, especially for late times. These two algorithms are, therefore, also considered here as benchmark comparisons for the inverse Laplace algorithm for transforming from the frequency to the time domain. Assuming an $e^{i\omega t}$ time dependence, the corresponding formulas for a causal step-off current source are (Newman et al., 1986) as follows:

$$\frac{\partial f(t)}{\partial t} = \frac{2}{\pi} \int_0^\infty \mathrm{Im}[F(\omega)] \sin(\omega t) \mathrm{d}\omega, \tag{8}$$

Table 1. An approximate analysis of cost and efficiency for the three inverse Laplace transform algorithms considered in this work (modified from Abate and Whitt, 2006). In the Gaver-Stehfest algorithm, we adopted the formula used by Everett (2009). The entries in the Gaver-Stehfest row have been changed accordingly.

Inversion algorithm	Number of function evaluations	System precision required, decimal digits (SP)	Number of correct digits produced (CD)	Efficiency (CD/SP)
Gaver-Stehfest	M	$1.1M$	$0.45M$	0.4
Euler	$2M + 1$	$1.0M$	$0.60M$	0.6
Talbot	M	$1.0M$	$0.60M$	0.6

$$\frac{\partial f(t)}{\partial t} = -\frac{2}{\pi}\int_0^\infty \mathrm{Re}[F(\omega)]\cos(\omega t)\mathrm{d}\omega, \qquad (9)$$

where $\mathrm{Im}[F(\omega)]$ and $\mathrm{Re}[F(\omega)]$ are the imaginary and real parts of the frequency-domain electric field or magnetic field, respectively, and $f(t)$ is the corresponding time-domain electric or magnetic field. If an $e^{-i\omega t}$ time dependence is chosen, the above two equations will have opposite signs (Key, 2012). In addition, for a step-on current, the transforms for $\partial f(t)/\partial t$ are the same as for the step-off current, but with opposite sign.

In our study, the formulations of the EM fields excited by a vertical magnetic dipole (VMD; as shown in Appendix A) and by a rectangular loop (as shown in Appendix B) are based on the $e^{i\omega t}$ time dependence, whereas the formulation of the electric field for the marine controlled-source electromagnetic (CSEM) example is based on the $e^{-i\omega t}$ time dependence (as shown in Appendix C). The cosine and sine transforms are computed here by the digital filtering lagged convolution method of Anderson (1983) with 787 coefficients and that of Key (2012) with 201 coefficients. In the following examples, all frequency-domain responses will be computed explicitly for Anderson's version, which is used as the benchmark; for Key's version, frequency-domain responses will be computed explicitly only at several tens of frequencies and then interpolated using cubic splines.

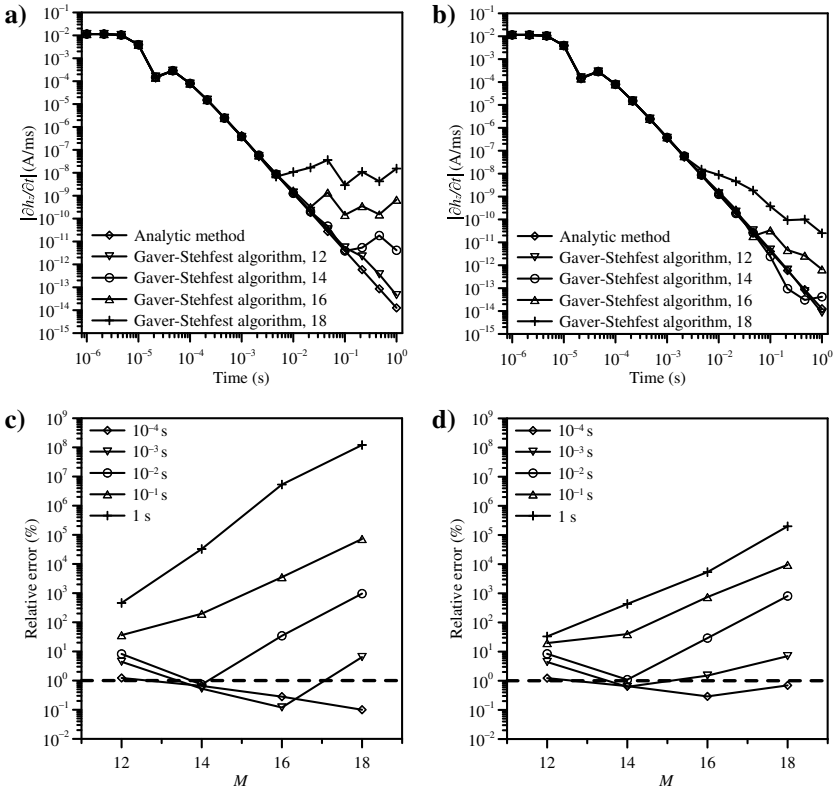

Figure 1. The $\partial h_z/\partial t$ excited at 100 m distance on a 100 Ωm half-space by a VMD calculated using double-precision arithmetic and varying M. Panels (a) and (c) are for calculations based on equation A-9; (b) and (d) are for calculations based on equation A-7. In (a) and (b), the symbols for all M values overlap at early observation times, whereas the symbols for all M values obviously deviate from the curve of the analytic solution (i.e., using equation A-10) at late times. In (c) and (d), the relative errors are with respect to the results of the analytic solution. The horizontal dashed lines indicate a relative error of 1%.

IMPROVING THE ACCURACY OF THE GAVER-STEHFEST ALGORITHM

Round-off errors arise in computations due to the intrinsic limitation of the finite precision representation of numbers and accumulate linearly in the course of subsequent numerical operations. To combat this limitation, Abate and Valkó (2004) use Mathematica, a mathematical computer environment that permits programming with multiprecision arithmetic, to develop numerical inverse Laplace transform algorithms. In general, double-precision arithmetic in a 64-bit computing environment provides at most 15 significant decimal digits for most programming languages, including Fortran and MATLAB. To implement variable-precision arithmetic, which allocates more than the usual bytes of memory for a specific number as directed, we used the Symbolic Toolbox contained in MATLAB. The specifications of the computer we used are Win7-64-bit operation system, Intel Core I3 2.4GHz CPU, and 4 GB of RAM.

VMD

We first investigate the use of variable-precision arithmetic in the computation of the Gaver-Stehfest algorithm for the time-derivative of the vertical magnetic field $\partial h_z(t)/\partial t$ resulting from a unit VMD on the surface of a homogeneous half-space. The offset between the VMD and the receiver is 100 m. For this scenario, the impulse response is calculated by the analytic method based on equation A-10 and the Gaver-Stehfest algorithm based on equations A-7 and A-9, the latter for better demonstration of the adverse effects caused by round-off errors. Equation A-9 includes the exponential term $e^{-\alpha s^{1/2}}$, which increases round-off errors over and above those coming from the Gaver-Stehfest algorithm itself in double-precision arithmetic, whereas equation A-7 does not include this exponential term, but rather the zeroth-order Bessel function of the first kind. To assess the performance of the Gaver-Stehfest algorithm, and based on the analysis of Abate and Whitt (2006), we set the significant decimal digits in the variable-precision environment to 32 for $10 \le M \le 28$, and to $[1.1M]$ for $30 \le M \le 48$. We then tested the effect of different selections of M.

Figures 1 and 2 show the impulse response calculated by double-precision arithmetic and variable-precision arithmetic respectively for this 100 Ωm homogeneous half-space example. In Figure 1, the accuracy gradually gets worse beyond 0.01 s, and the impulse responses for all M obviously deviate from the analytic solution at late times, especially for the responses based on equation A-9. On the contrary, the impulse responses calculated using variable-precision arithmetic (Figure 2) exhibit good accuracy at all times except for at low and high M values. In Figure 2a and 2b, with increasing M, the accuracy improves until $M = 28$, and then it degrades from $M = 32$ to 48. For M larger than 32, the poorer accuracy is attributed to the Gaver-Stehfest algorithm itself. In Figure 2c

and 2d, the significant decimal digits in the variable-precision environment were set to 32, 40, $[1.1M]$, and $[2.2M]$ for $M = 48$. For the late times, the relative errors for the decimal digits equal to 32 are much larger than the corresponding errors for the other three values, for which the relative errors agree well with each other. It suggests that round-off errors are not responsible for the relatively poor accuracy for M larger than 32 in Figure 2a and 2b. Furthermore, this example demonstrates that given a specific geoelectric model, the Gaver-Stehfest algorithm is valid only for a limited range of M values.

As expected, the accuracies of the impulse responses calculated by equation A-9 (Figure 1a and 1c) are worse than those calculated using equation A-7 (Figure 1b and 1d) in double-precision arithmetic, whereas the accuracies of both equations are approximately equal using variable-precision arithmetic except for earlier times, when A-9 benefits from a greater M (shown in Figure 2). Regarding the efficiency of variable-precision arithmetic, the computation times using equation A-7 were, for example, 230 and 470 s for $M = 16$ and 32, respectively. When using equation A-9, the times were 8 and 13 s for $M = 16$ and 32. The substantial difference in computing times between equations A-7 and A-9 is caused by the Hankel transform used to solve the integral expression including the zeroth-order Bessel function of the first kind. Here, a 120-coefficient Hankel transform was used (Guptasarma and Singh, 1997), meaning that 120 expressions had to be calculated to solve for equation A-7, whereas only one was required for equation A-9.

Reference values

In general, there is no analytic solution available for stratified media and for loop and grounded sources. Before proceeding, we investigate calculating reference values using a numerical approach. In this study, we considered two versions of cosine and sine digital filtering algorithms: one by Anderson (1983) that has 787 coefficients and one by Key (2012) that has two possible sets of coefficients (101 and 201 coefficients). When using Anderson's version, for which all frequency-domain values were computed explicitly, the maximum observation time was set to 2 s and the number of lagged convolutions was set to 150. For Key's version, we chose the 201-coefficient cosine and sine transforms. For example, the frequency-domain values were explicitly computed at 85 frequencies, distributed from 10^{-3} to 10^{9} Hz with seven frequencies per decade, and then interpolated to the 201 required frequencies using cubic spline interpolation.

We investigate the performance of these transforms for two homogeneous half-spaces of 100 and 1000 Ωm using equation A-7. As expected, the cosine and sine transforms with 787 coefficients exhibit better accuracy for both half-space conductivities considered (Figure 3). It is not surprising that the efficiency is relatively low for the 787-coefficient transforms. For example, the computation time for this example is 1.3 s, whereas it is 0.1 s for the 201-point transforms with frequency-domain responses explicitly computed at 85 frequencies with subsequent interpolation. In this paper, we mainly focus on accuracy; hence, we choose the cosine transform with 787 coefficients in the following sections as the standard against which we compare the various inverse Laplace transform algorithms.

Loop source

We now consider the variable-precision arithmetic version of the Gaver-Stehfest algorithm for the loop source scenario. Please refer to Appendix B and the specific expressions therein that were used to obtain the numerical results. The sizes of the transmitting loop considered are 5×5, 100×100, and 1000×1000 m, with the receiver always located at the center of the loop. The observation times used here are those for the 30/25 Hz setting of the Geonics Protem system. These times correspond to 20 gates, ranging from 88.13 μs to 6.978 ms (Woods, 2006). Values of $M = 12$, 14, 16, and 18 were considered for the Gaver-Stehfest algorithm. The desired number of significant decimal digits was set to 32 when using variable-precision arithmetic. For this example, the computed value is the time-derivative of the vertical magnetic induction $\partial b_z(t)/\partial t$ for a step-off transmitter waveform.

Figure 4 shows the results calculated using the Gaver-Stehfest algorithm for the 1000 Ωm half-space and the corresponding rela-

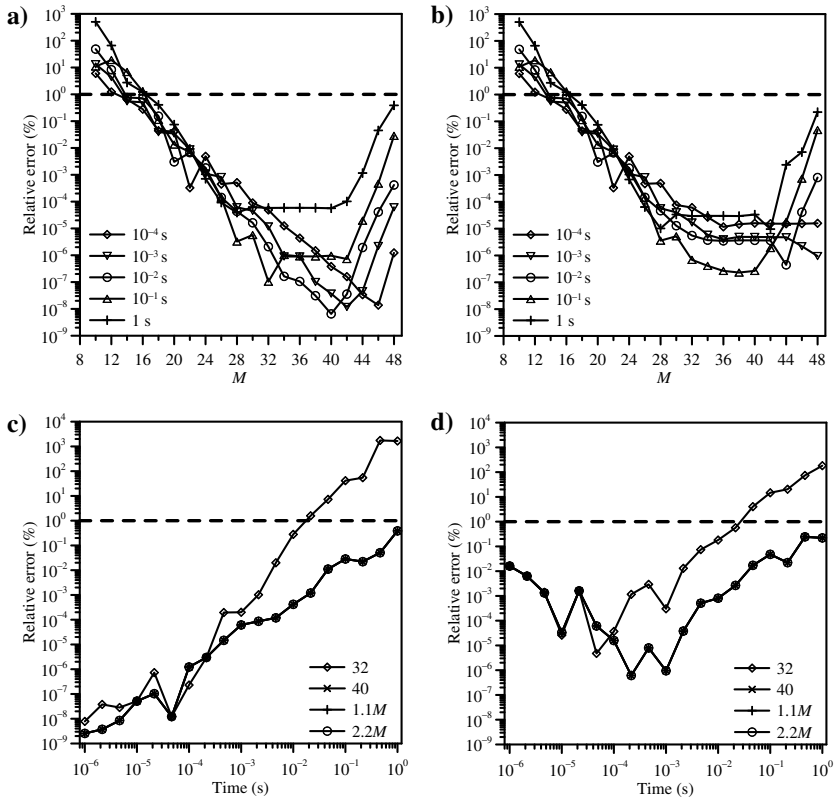

Figure 2. The relative errors in values of $\partial h_z/\partial t$ at a distance 100 m for a VMD on the surface of a 100 Ωm half-space when compared with the analytic solution based on equation A-10 using variable-precision arithmetic and varying M. Panels (a) and (c) are for calculations based on equation A-9; (b) and (d) are for calculations based on equation A-7. Panels (c) and (d) show the relative errors of all observation times for $M = 48$ using variable-precision arithmetic with 32, 40, $[1.1M]$ and $[2.2M]$ significant decimal digits. The horizontal dashed lines indicate the 1% relative error level.

Figure 3. The relative errors between the analytic solution based on equation A-10 and the numerical solutions based on equation A-7 for the impulse response (i.e., $\partial h_z/\partial t$ for a step-off waveform) excited by a VMD source for half-spaces of 100 Ωm (a) and 1000 Ωm (b). The horizontal dashed lines indicate a relative error of 1%.

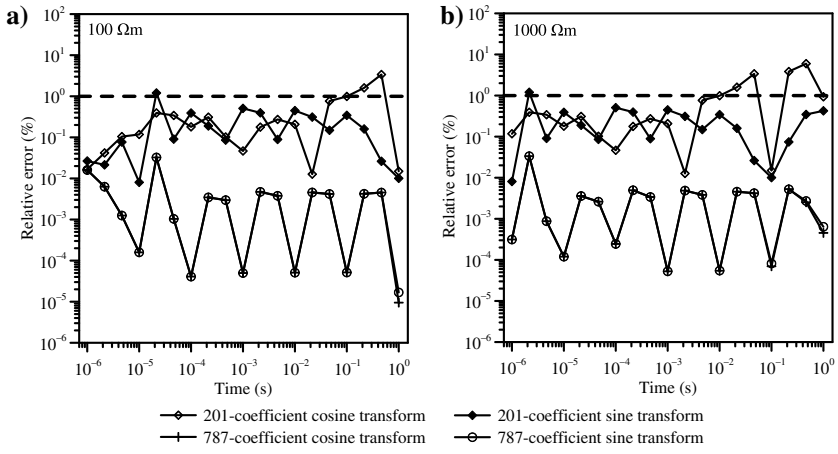

Figure 4. The values of $\partial b_z/\partial t$ at the center of a transmitting loop laid on the surface of a 1000 Ωm half-space. Panels (a) and (b) are for a 5×5 m loop, (c) and (d) are for a 100×100 m loop, and (e) and (f) are for a 1000×1000 m loop. In (d) and (f), the horizontal dashed line indicates a relative error of 1%.

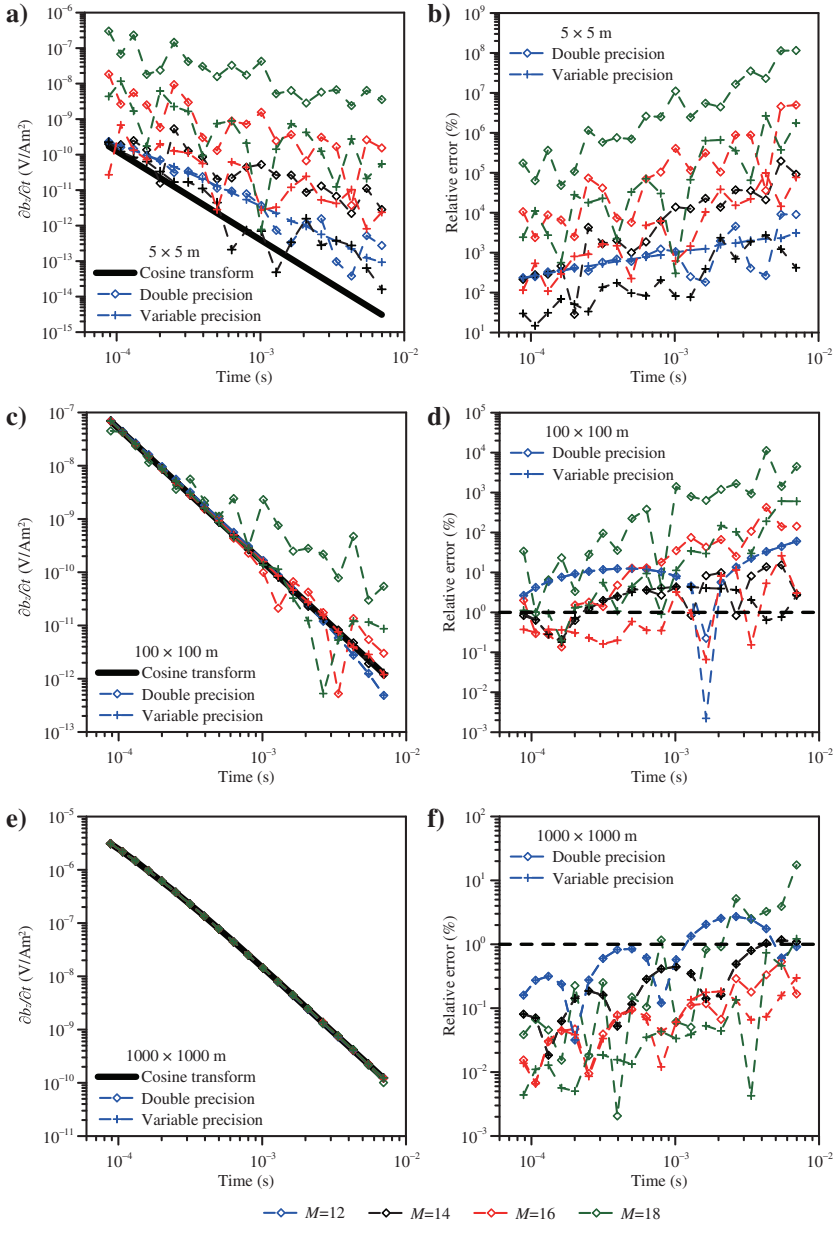

tive errors compared with the 787-coefficient cosine transform. For the 5×5 m loop, the Gaver-Stehfest algorithm with 12, 14, 16, and 18 coefficients cannot obtain accurate solutions in double- or variable-precision arithmetic. For the 100×100 m loop, the relative errors are generally smaller, especially for the early observation times in variable-precision arithmetic. For the 1000×1000 m loop, most of the relative errors are smaller than 1%, except for the ones at late times for the 12- and 18-coefficient Gaver-Stehfest algorithm. These examples demonstrate that the accuracy of the Gaver-Stehfest algorithm is severely problem dependent.

Figure 4 also shows that the responses calculated using variable-precision arithmetic are more accurate than those using double-precision arithmetic. In these examples, round-off errors not only originate from the Gaver-Stehfest algorithm, but also from the Laplace-domain formulas. If the EM field is very weak, as is the case at late times and low frequencies, the round-off errors associated with the Laplace-domain calculations will have a distinct effect on the numerical solutions. For example, the responses for the 5×5 m loop calculated by the 12-coefficient Gaver-Stehfest algorithm, which should be free of round-off errors as analyzed above (see Table 1), exhibit obvious errors at late times.

In spite of the good accuracy provided by variable-precision arithmetic for the Gaver-Stehfest algorithm for some situations, the computation times are unaffordable in the context of forward modeling and inverting geophysical EM data. For example, the computation times for the above example (regardless of loop size) were 2665, 3116, 3552, and 4208 s for $M = 12$, 14, 16, and 18, respectively. Hence, we now investigate alternative algorithms for implementing inverse Laplace transforms.

ACCURACY TESTING OF THE EULER AND TALBOT ALGORITHMS

As stated above, the Euler and Talbot algorithms are able to provide more accurate solutions in a fixed-precision computing environment than the Gaver-Stehfest algorithm. To test their performance for typical EM geophysics situations, we consider the time-domain responses for central-loop and fixed-loop configurations based on the expressions presented in Appendix B, and for a horizontal electric dipole (HED) source in a marine CSEM scenario based on the expressions presented in Appendix C, using double-precision arithmetic.

Central-loop configuration

First, we investigate applications of these two algorithms to half-space models of 200, 500, 1000, and 2000 Ωm for the central-loop configuration. The candidate M range is chosen to be from 2 to 24 for the Euler algorithm, and from 8 to 48 for the Talbot algorithm. The transmitting loop sizes are 5×5, 10×10, 20×20, 50×50, and 100×100 m.

Figure 5 shows the impulse response $\partial b_z(t)/\partial t$ for a step-off transmitter waveform computed using the Euler and Talbot algorithms with different values of M for 5×5 and 100×100 m loops. The observation times are those for the 30/25 Hz Geonics Protem system. In Figure 5a and 5b, we can see that impulse responses for parts of the ranges of M that were considered agree well with the 787-coefficient cosine transform solutions for both loops and both algorithms. Compared with the results for the Gaver-Stehfest algorithm using both double- and variable-arithmetic (see in Figure 4), the Euler and Talbot algorithms give better accuracy for this model. The characteristics of the relative errors for these two algorithms with different values of M for the observation time of 0.007 s are shown in Figure 4c and 4d. This observation time is approximately the latest time recorded by the 30/25 Hz Geonics Protem system. This relatively late time is also where the methods considered here first begin to struggle. As M increases for both algorithms, the relative errors decrease rapidly for both loop sizes and then increase smoothly. An obvious characteristic is that the relative errors do not change for the different loops when using the Euler algorithm with smaller M values.

Tables 2 and 3 summarize the ranges of M for which the relative errors at 0.007 s are smaller than 1% compared with the 787-coefficient cosine transform. We can see that, as the resistivity of the half-space increases or the loop size decreases, the range of M that gives better than 1% accuracy narrows. This demonstrates that the Euler and Talbot algorithms are also problem despendent just like the Gaver-Stehfest algorithm. However, these two algorithms nevertheless generate accurate time-domain values, except perhaps for

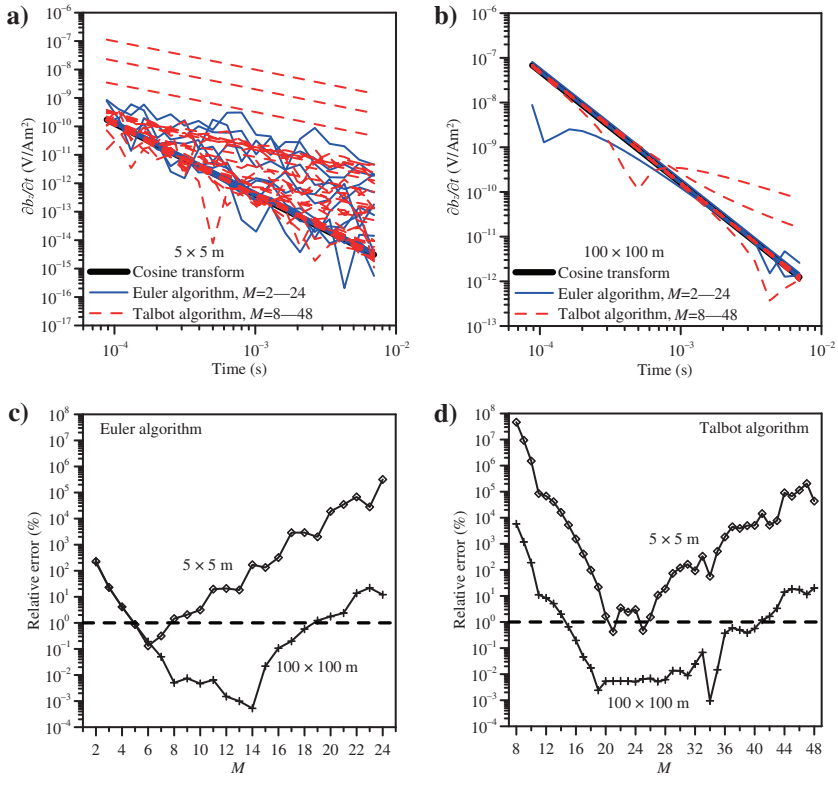

Figure 5. For the central-loop configuration for 5×5 and 100×100 m loops, the $\partial b_z/\partial t$ values computed by the Euler ($M = 2 - 24$) and Talbot ($M = 8 - 48$) approaches (a) and (b). The relative errors for these two approaches were compared with the 787-coefficient cosine transform at 0.007 s (c) and (d). The model was a half-space of 1000 Ωm.

small loops on resistive half-spaces (e.g., 5×5 m and 2000 Ωm) using the Talbot algorithm. As Tables 2 and 3 also show, the minimum M that gives <1% relative errors varies with the loop size and the half-space resistivity for the Talbot algorithm, but it is always 6 for the Euler algorithm. Therefore, the Euler algorithm is more appropriate for the central-loop configuration in the aspect of robustness of choosing M.

Next, we applied the Euler and Talbot algorithms to stratified models. The observation times considered are again those for the 30/25 Hz Geonics Protem system. The geoelectric models and the corresponding results are shown in Table 4 and Figure 6, respectively. For model 1, the M value was chosen to be the minimum in the ranges given in the fourth rows in Tables 2 and 3 for the Euler and Talbot algorithms, repectively. The M value for model 2 was taken from the first rows in Tables 2 and 3. These choices were based on the basement resistivity of the two models. The 787-coefficient cosine transform is again used for comparison here. As shown in Figure 6a and 6c, the responses computed by the three methods agree well. In Figure 6b and 6d, the average relative error of the Euler algorithm is obviously larger than that of the Talbot algorithm, which benefits from the larger number of evaluations implemented in the Laplace domain, but it demands more computation time. For model 1, all the relative errors are below 1% for these two Laplace inversion algorithms. For model 2, the relative errors at several intermediate times are slightly larger than 1% when using the Euler algorithm, but are otherwise less than 1%.

Table 2. The M ranges for which the relative errors at 0.007 s for the central-loop configuration are smaller than 1% when using the Euler algorithm, compared with the 787-coefficient cosine transform. The range of values of M that were tested was from 2 to 24. Homogeneous half-space models were considered.

Resistivity (Ωm)	5×5 m	10×10 m	20×20 m	50×50 m	100×100 m
200	6–10	6–13	6–17	6–18	6–22
500	6–9	6–11	6–15	6–17	6–21
1000	6–7	6–9	6–14	6–16	6–18
2000	6–7	6–9	6–11	6–14	6–17

Table 3. Same as Table 2, but for the Talbot algorithm. The range of M values tested was from 8 to 48.

Resistivity (Ωm)	5×5 m	10×10 m	20×20 m	50×50 m	100×100 m
200	20–24	19–28	17–35	15–40	12–44
500	20–21	19–26	18–30	16–37	14–41
1000	21, 25	20–23	19–28	17–35	15–40
2000	—	20–21	19–26	18–32	16–37

Table 4. The resistivities and thicknesses of the three-layer models considered in this paper.

Model	First resistivity (Ωm)	Second resistivity (Ωm)	Third resistivity (Ωm)	First thickness (m)	Second thickness (m)
Model 1	100	10	1500	100	50
Model 2	50	1000	100	50	500

Fixed-loop configuration

We also investigate applications of the Euler and Talbot algorithms to fixed-loop configurations. We first consider the half-space models mentioned above. The side length of the transmitting loop is 1000 m. The x-coordinates of the receiver locations are 0, 100, 200, 300, and 400 m (relative to the loop center), with the y-coordinate equal to 0 m. The observation time is chosen as 0.07 s, which is essentially equal to the last observation time for the 3.0/2.5 Hz setting of the Geonics Protem system.

Figure 7 shows the relative errors in the impulse responses computed using different values of M. As M increases, the relative errors for all x-coordinates decrease sharply before leveling off for the Euler and Talbot algorithms with a slight increase for the largest values of M. As shown in Tables 5 and 6, the M ranges that gave relative errors less than 1% for half-spaces of different resistivities follow the same general pattern as for the central-loop configuration. One difference between these two configurations, however, is that the M ranges are broader for the fixed-loop configuration due to the larger size of the transmitter loop considered for this example. The M ranges show very little fluctuation as the x-coordinate of the receiver changes, except for the 2000 Ωm half-space model. In this situation, the M range gets broader as the x-coordinate increases, that is, as the observation point moves from the loop center to near the loop edge.

We next investigate the performance of these two algorithms for the fixed-loop configuration for stratified models. The minimum M value was chosen based on Tables 5 and 6. The M value was, therefore, always set to 6 for the Euler algorithm, whereas for the Talbot algorithm the chosen M was 12 for model 1 and 10 for model 2. Observation times ranging from 90 μs to 69.78 ms, which correspond to 30 time gates of the 3.0/2.5 Hz Geonics Protem system (Woods, 2006), were considered. As can be seen from Figures 8a, 8c, 9a, and 9c, the results calculated by the Euler and Talbot algorithms agree well with those of the 787-coefficient cosine transform for all observation points and times. As for the relative errors, only the values at the last six times are larger than 1%, and only just, for model 1 when using the Euler algorithm. The Talbot algorithm gives the smaller average relative errors in general.

As for the central-loop configuration, one distinct advantage of the Euler algorithm is the robustness of choosing a suitable M, which was always 6 in these studies. For the Talbot algorithm, the minimum M varies with loop size and resistivity, but this algorithm does give the smaller average relative errors.

HED

One of the main contemporary applications for an HED source is in marine CSEM. Here, we use the canonical 1D reservoir model of Constable and Weiss (2006) as our example. This model comprises: air (10^{-12} Ωm, infinity), seawater (0.3 Ωm, 10^3 m), seabed (1 Ωm,

10^3 m), hydrocarbon reservoir (10^2 Ωm, 10^2 m), and basement (1 Ωm, infinity). The HED source is placed at 10 m above the water bottom, and the receiver offsets are 1, 2, 3, 5, 10, and 15 km. For this example, the values of M that were investigated ranged from 2 to 15 for the Euler algorithm and from 5 to 30 for the Talbot algorithm. The 787-coefficient cosine transform is again used for comparison.

Figure 10 shows the relative errors for various receiver offsets and various values of M for an observation time of 0.1 s. The relative errors for all offsets decrease first as M increases for the Euler and Talbot algorithms before increasing. The exception is the $r = 1$ km situation, for which the errors do not increase for larger values of M. The M ranges for which relative errors are smaller than 1%, for a selection of observation times, are shown in Tables 7 and 8. For observation times of 1–100 s the minimum M that gives relative errors less than 1% is 3–6 for all six offsets for the Euler algorithm and 5–10 for all offsets for the Talbot algorithm. For 0.01 and 0.1 s, the electric field is too weak to calculate accurately at large offsets due to the low diffusing velocity of EM fields in a conductive environment. The Talbot algorithm does obtain an accurate solution at offsets of 1 and 2 km for 0.01 s, and 3 km for 0.1 s, but the Euler algorithm does not. The Talbot algorithm is, therefore, somewhat more appropriate for this scenario in terms of efficiency and accuracy.

Figure 11 shows the time derivative of the inline horizontal electric field $\partial e_h(t)/\partial t$ for a step-off transmitter waveform computed using M values chosen on the basis of the above analysis. A value of $M = 7$ was used for the Euler algorithm, and it was $M = 11$ for the Talbot algorithm. As the receiver offset increases, the responses tend to be inaccurate at early observation times, but they coincide well with each other at late times. For this model, we also calculated the impulse responses by the 201- and 787-coefficient cosine and sine transforms, for which the frequency-domain responses were explicitly computed at several tens of frequencies and then interpolated using cubic splines. Figure 12 shows the comparison between these responses and those for the Euler ($M = 7$) and Talbot ($M = 11$) algorithms. The relative errors are calculated based on the values obtained by the 787-coefficient cosine transform for which all frequency-domain responses were computed explicitly (see Figure 11). For the splined cosine and sine transforms, the frequency-domain responses were explicitly computed for 41 or 161 frequencies distributed from 10^{-4} to 10^4 Hz with 5 or 20 frequencies per decade. For the case of 41 frequencies, the Euler and Talbot algorithms exhibit much better accuracy than the splined cosine and sine transforms with 201 and 787 coefficients, whereas for the case of 161 frequencies, the curves for the six computed responses are intermixed with each other. At early times, the splined

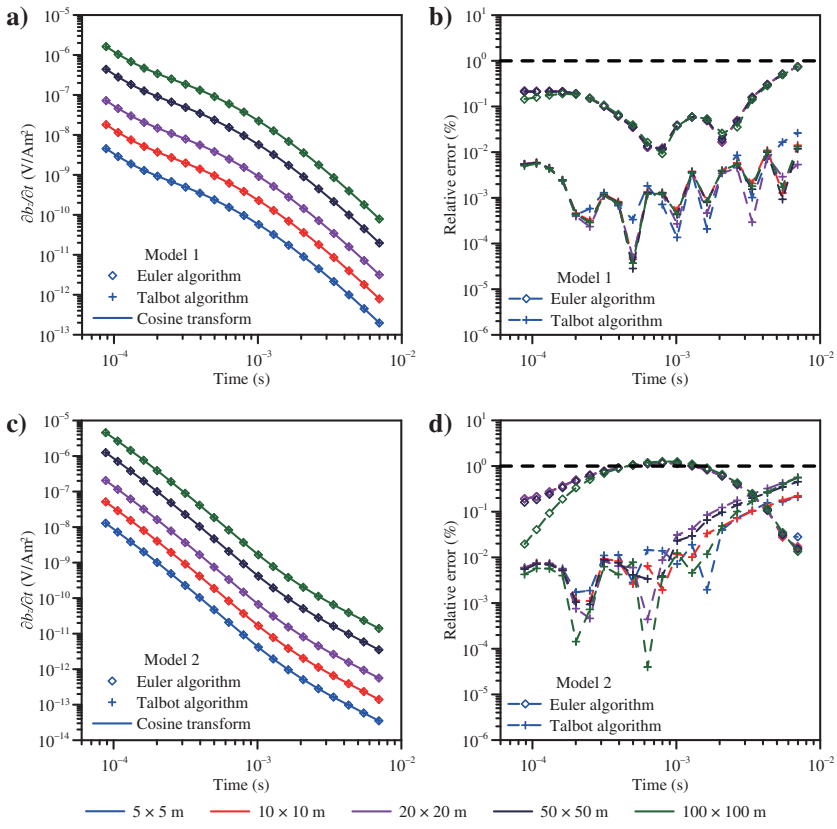

Figure 6. The values of $\partial b_z/\partial t$ and relative errors for the central-loop configuration for the stratified models given in Table 4. Here, the M value is always six for the Euler algorithm; for the Talbot algorithm, the M value of every model is chosen as the minimum value of the ranges given in Table 3 using the fourth row for model 1 and the first row for model 2. Panels (a) and (b) are for model 1; (c) and (d) are for model 2. In (b) and (d), the dashed lines indicate a relative error of 1%.

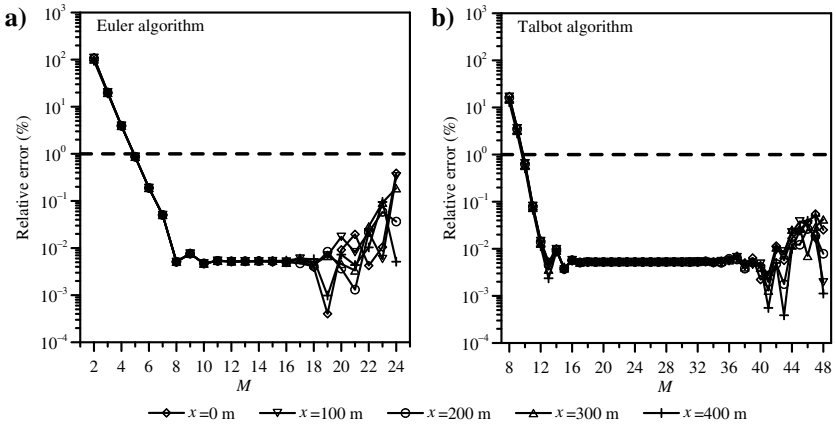

Figure 7. The relative errors in the impulse response for the fixed-loop configuration calculated using the (a) Euler and (b) Talbot algorithms and for varying separation between receiver and loop center. The relative error is with respect to the 787-coefficient cosine transform. The model here is a half-space of 200 Ωm, and the observation time is 0.07 s.

Table 5. The M ranges for obtaining relative errors smaller than 1% for 0.07 s for the fixed-loop configuration when using the Euler algorithm. Relative errors are with respect to the 787-coefficient cosine transform. The tested M range was from 2 to 24. Homogeneous half-space models were used.

Resistivity (Ωm)	$x = 0$ m	$x = 100$ m	$x = 200$ m	$x = 300$ m	$x = 400$ m
200	6–24	6–24	6–24	6–24	6–24
500	6–24	6–24	6–24	6–24	6–24
1000	6–22	6–22	6–22	6–22	6–22
2000	6–21	6–23	6–24	6–22	6–22

Table 6. Same as Table 5, but for the Talbot algorithm. The tested M range was from 8 to 48.

Resistivity (Ωm)	$x = 0$ m	$x = 100$ m	$x = 200$ m	$x = 300$ m	$x = 400$ m
200	10–48	10–48	10–48	10–48	10–48
500	11–48	11–48	11–48	11–48	11–48
1000	11–48	11–48	11–48	11–48	11–48
2000	12–45	12–45	12–45	12–46	12–46

201-coefficient transforms have the worst accuracy, whereas the splined 787-coefficient ones do not present more accurate solutions than the other algorithms.

EFFICIENCY COMPARISON

The efficiency of an algorithm for computing an inverse Laplace transform is critical to its usefulness. In this section, we assess the computation times required by the Gaver-Stehfest, Euler and Talbot algorithms in terms of the parameter M, and compare these times with those for the cosine and sine transforms.

For a specific comparison, we consider the 1000 Ωm half-space model for a 1000×1000 m loop and central-loop configuration (see above). We consider computing values of $\partial b_z(t)/\partial t$ at 20 and 30 observation times for the range shown in Figure 4 for a step-off transmitter current. We consider the 787-coefficient cosine transform with explicit computation of all the required frequency-domain responses and the 201-coefficient sine transform for which frequency-domain responses were explicitly computed at 41 and 161 frequencies distributed from 10^{-1} to 10^{7} Hz, respectively. For these three transform methods, the computation time is essentially independent of the number of observation times by design of the lagged algorithm. For the three Laplace inversion algorithms, a range of values of M was again investigated. Given M, there are $2M + 1$ Laplace-domain evaluations needed for the Euler algorithm and M for the Gaver-Stehfest and Talbot algorithms (Table 1).

As shown in Figure 13, the 201-coefficient splined sine transform is the most efficient method: For the 20 and 30 observation times, its computation times are equal to 0.15 and 0.56 s, respectively, for the versions with 41 and 161 responses computed explicitly. The

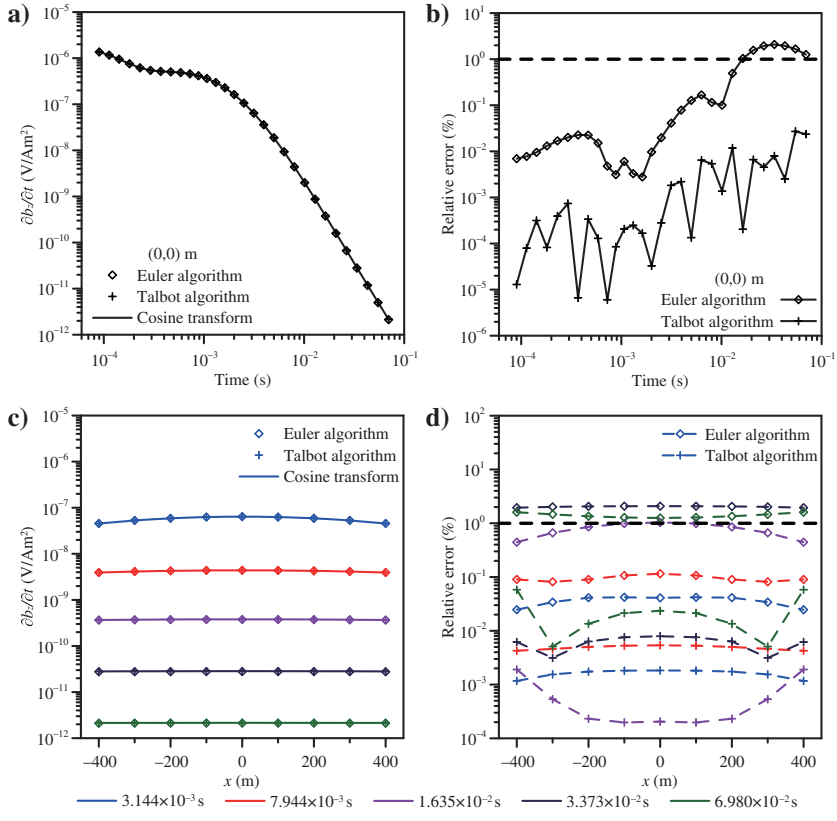

Figure 8. The values of $\partial b_z/\partial t$ for the fixed-loop configuration (transmitter loop 1000×1000 m) for model 1. The solid lines represent the results computed by the 787-coefficient cosine transform, and the circles and crosses denote the results computed using the Euler ($M = 6$) and Talbot ($M = 12$) algorithms. The results for the observation point (0,0) m are shown in (a) and (b). The results of nine observation points ($y = 0$ m) are shown in (c) and (d). In (b) and (d), the horizontal dashed lines indicate a relative error of 1%.

Gaver-Stehfest algorithm in variable-precision arithmetic is, not surprisingly, the most inefficient method. The 787-coefficient cosine transform with explicit evaluation of frequency-domain responses is the second most computationally expensive, taking 4 s for 20 and 30 observation times. The computation times for the Gaver-Stehfest, Euler, and Talbot algorithms in double-precision arithmetic grow linearly as M increases. However, their computation times are all between 0.6 and 4 s. Due to only real operations being required, the Gaver-Stehfest algorithm is faster than the Talbot algorithm for the same M in double-precision arithmetic. Based on the accuracy analysis in Tables 5 and 6, the minimum values of M giving relative errors less than 1% for the Euler and Talbot algorithms would be 6 and 11, for example. The corresponding computation times for the Euler and Talbot algorithms are 1.0 and 0.8 s for 20 observation times, and 1.4 and 1.1 s for 30 observation times.

DISCUSSIONS

In this section, we will discuss two points: One is choosing M for the Euler and Talbot algorithms, and the other is to make comparisons between spectral methods used in 3D forward modeling.

Choosing M for the Euler and Talbot algorithms

In general, there is no definitive method for knowing the optimal M value for an inverse Laplace transform algorithm that simultaneously achieves good accuracy and efficiency. However, based on the work presented in this paper, we can anticipate the minimum M required for a sufficiently accurate Laplace inversion for typical geophysical EM scenarios by considering the following points:

1) For a loop source, and especially for the observation location at the loop center, the time-domain responses at late times are always more difficult to calculate accurately than those at early times because of the movement of the induced currents downward and outward and their decay. Therefore, we should concentrate on the behavior of the responses at late times when choosing M. For the marine CSEM scenario, however, it is just the opposite: The time-domain responses are extremely weak at early times for long offsets.
2) If an M value is good for calculating the time-domain responses for a resistive medium, it will also be applicable to more conductive mediums for which the decay with respect to time is less. Given a stratified model for a loop source scenario, the M value should be determined according to the basement resistivity, on which the time-domain response at late times largely depends.
3) Similarly, a smaller loop always induces weaker EM responses than larger ones. Therefore, calculating time-domain responses for a smaller loop always requires a larger M value.

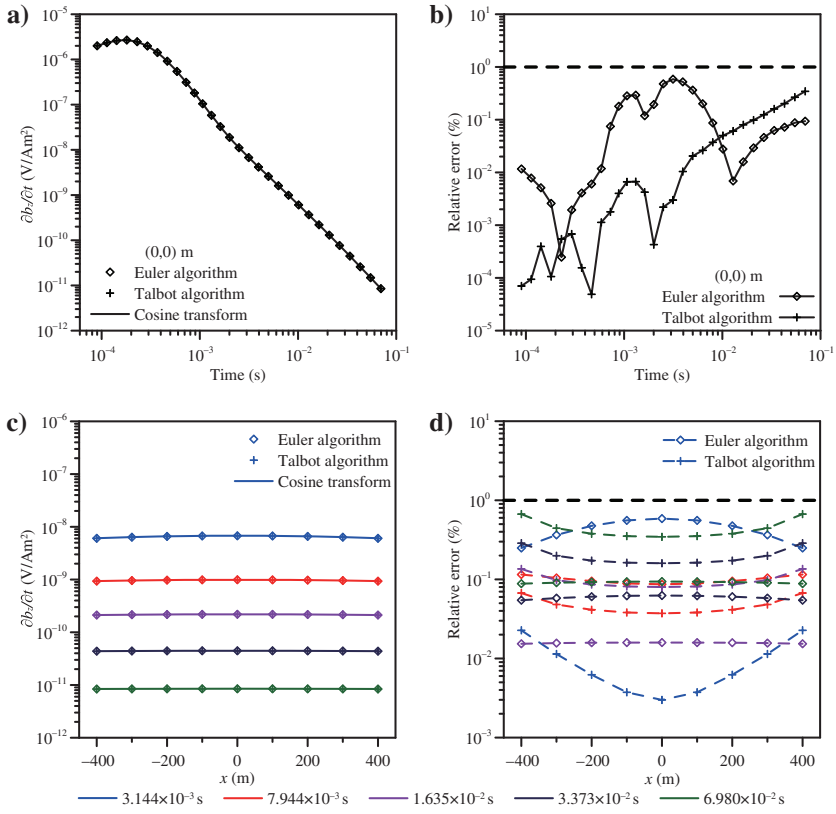

Figure 9. Same as Figure 8, but for model 2. The M value is six for the Euler algorithm and 10 for the Talbot algorithm.

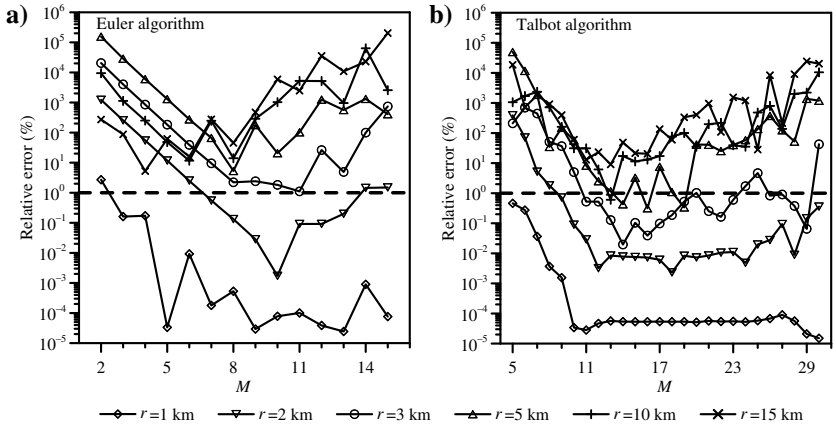

Figure 10. The relative errors for the marine CSEM scenario for varying the offset r compared with the 787-coefficient cosine transform. The model is the canonical 1D reservoir model of Constable and Weiss (2006), and the observation time is 0.1 s. Panels (a) and (b) are for the Euler and Talbot algorithms, respectively.

The above guidelines have been tested on stratified models for central- and fixed-loop configurations. Choosing M based on these guidelines cannot guarantee that the relative errors at all times are less than the desired error floor, but this avoids having to determine the minimum M by trial and error for each new model and situation.

Table 7. The M ranges giving relative errors less than 1% (relative to the 787-coefficient cosine transform) for the marine CSEM example using the Euler algorithm. The range of values of M tested was from 2 to 15. The 1D canonical reservoir model of Constable and Weiss (2006) was used.

Observation time (s)	$r = 1$ km	$r = 2$ km	$r = 3$ km	$r = 5$ km	$r = 10$ km	$r = 15$ km
10^{-2}	—	—	—	—	—	—
10^{-1}	3–15	7–13	—	—	—	—
1	3–15	4–15	4–15	4–15	4–15	4–15
10^{1}	5–15	5–15	3–15	3–15	3–15	3–15
10^{2}	6–15	6–15	6–15	5–15	5–15	4–15

Table 8. Same as Table 7, but for the Talbot algorithm. The tested values of M ranged from 5 to 30.

Observation time (s)	$r = 1$ km	$r = 2$ km	$r = 3$ km	$r = 5$ km	$r = 10$ km	$r = 15$ km
10^{-2}	17–19	17	—	—	—	—
10^{-1}	5–30	9–30	11–23	14, 16	—	—
1	5–30	6–30	6–30	5–30	5–30	5–30
10^{1}	7–30	5–30	5–30	5–30	5–30	5–30
10^{2}	10–30	9–30	8–30	7–30	5–30	5–30

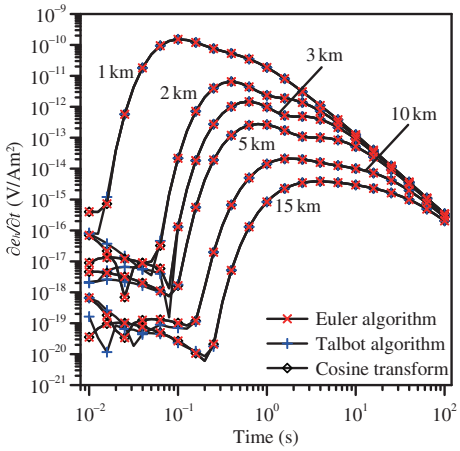

Figure 11. Values of $\partial e_h/\partial t$ for the canonical 1D reservoir model for a step-off source and varying source-receiver offsets. The responses were computed by the Euler ($M = 7$) and Talbot ($M = 11$) algorithms, and the 787-coefficient cosine transform for which all frequency-domain responses were explicitly computed.

Finally, we recommend the Euler algorithm for computing time-domain responses for central- and fixed-loop configurations due to the robustness of choosing M and the Talbot algorithm for the marine CSEM scenario due to its better accuracy for this case as illustrated above. Furthermore, good, general values of M for the Euler and Talbot algorithms, certainly in terms of initial values to try, are 7 and 15, respectively, which are the maximum values free of round-off errors for these two algorithms in a computing environment of 15 decimal digits.

Spectral methods in 3D forward modeling

Spectral methods, based on the cosine and sine transforms or inverse Laplace transform algorithms, have been widely used in 3D forward modeling for calculating time-domain EM responses.

For the cosine and sine transforms using a lagged-convolution digital filtering method, the computational expense mainly depends on the number of frequencies as determined by the range of observation times rather than the number of observation times. Hence, these two transforms are particularly applicable to situations with dozens of observation times. However, a time-domain response for any time relies on the freqency-domain responses of all frequencies for these two transforms. In other words, an inaccurate frequency-domain response can affect the time-domain responses for all observation times. In 3D forward modeling, it is hard to obtain accurate solutions for high frequencies due to numerical dispersion and for low frequencies due to the difficulties of solving the necessary linear systems of equations by an iterative method. To improve numerical accuracy, finer grids or higher order numerical methods are used to alleviate numerical dispersion for high-frequency situations, and iterative methods combined with a divergence correction or direct solvers are used to solve the linear system of equations for low-frequency situations. As a result, more computational time is required. When using inverse Laplace transform algorithms, a time-domain response for any time is calculated based on more or less a dozen Laplace-domain responses relating to this time. Therefore, an inaccurate Laplace-domain response only affects the time-domain response for the corresponding observation time instead of all times.

In general, Laplace transform algorithms have lower efficiency for typical EM geophysics situations than cosine and sine transforms. Taking the marine CSEM scenario used in the above section as a example, the number of responses evaluated in the Laplace domain is 15 and 11 per observation time for the Euler ($M = 7$) and Talbot ($M = 11$) algorithms, respectively. If there are 20 observation times, 300 and 220 Laplace-domain responses are required. Supposing the splined cosine and sine transforms are required to keep the same accuracy with the Euler and Talbot algorithms, the number of frequencies should be approximately 20 per decade based on the accuracy comparison in Figure 12. If the frequency range extends across eight magnitudes from 10^{-4} to 10^{4} Hz, the number of evaluations in the frequency domain will be only 161.

As analyzed and discussed above, spectral methods based on the cosine and sine transforms and inverse Laplace transform algorithms have their own advantages and disadvantages. For a particular problem, one should choose an appropriate method based on the number and range of observation times. In addition to the time-stepping method, spectral methods based on the cosine and sine transforms are currently in a position of dominance for 3D time-domain forward modeling. However, spectral methods based on the inverse Laplace transform algorithms can be competitive in terms of accuracy and efficiency and so deserve more attention in the future.

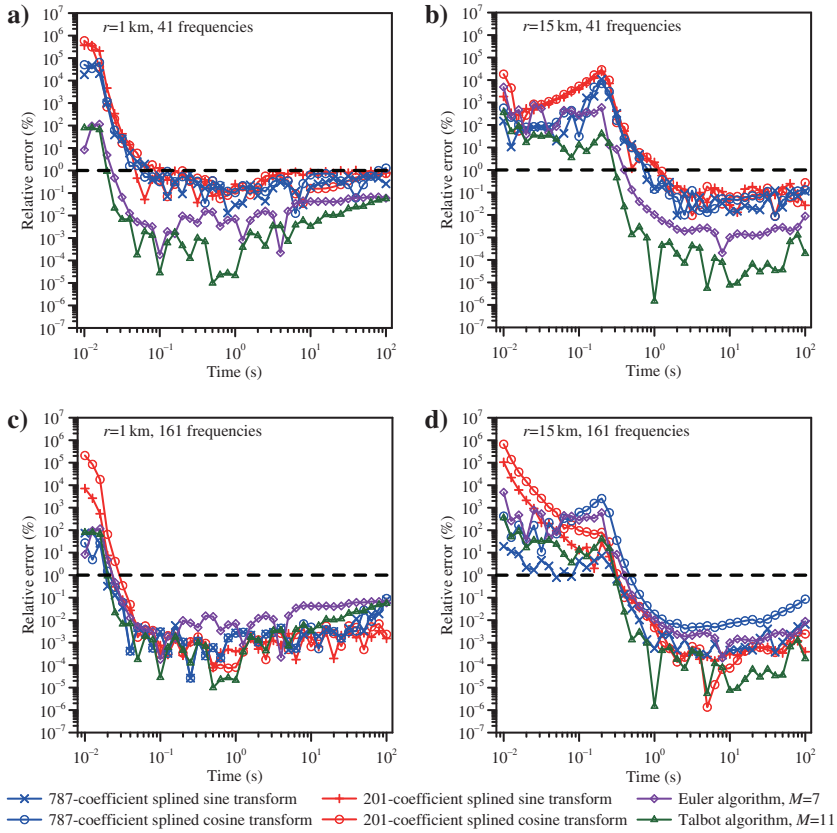

Figure 12. An accuracy comparison for the marine CSEM scenario between the cosine and sine transforms using 787 and 201 coefficients but with splined frequency-domain responses and the Euler ($M = 7$) and Talbot ($M = 11$) algorithms. Actual frequency-domain responses were computed at 41 frequencies in (a) and (b); 161 frequencies were used in (c) and (d).

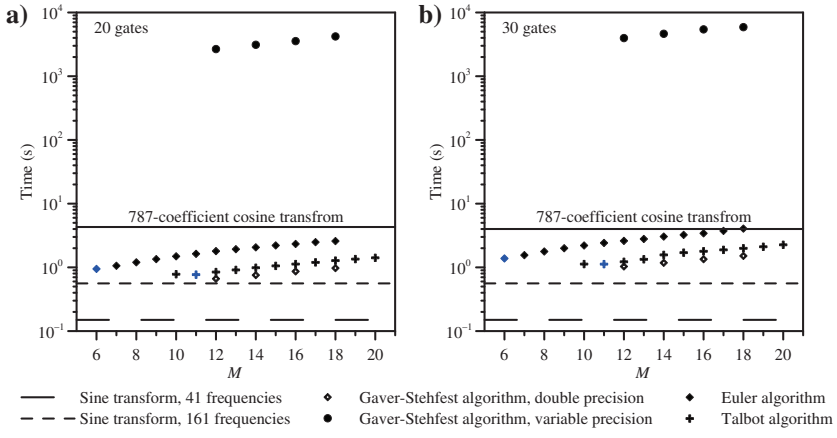

Figure 13. The computation times for the Gaver-Stehfest, Euler, and Talbot algorithms as functions of parameter M. Panels (a) and (b) are for 20 and 30 observation time gates, respectively, which are typical of the Geonics Protem system. The blue symbols correspond to the minimum values of M giving relative errors less than 1% as shown in Tables 5 and 6.

CONCLUSIONS

This paper considered the feasibility of improving the accuracy of the Gaver-Stehfest algorithm using variable-precision arithmetic for computing the inverse Laplace transform, which is one means of computing time-domain EM responses, and then we presented two other possible algorithms, namely, the Euler and Talbot algorithms. The Gaver-Stehfest algorithm using variable-precision arithmetic in the MATLAB programming environment is able to compute the required time-domain responses accurately. However, its computational expense makes it unsuitable for our applications. As effective alternatives to the Gaver-Stehfest algorithm, the Euler and Talbot algorithms can provide the desired accuracy and are less problem dependent. When using double-precision arithmetic, they clearly have higher accuracy than the Gaver-Stehfest algorithm, particularly at late observation times for loop sources. As for their efficiency, the Euler and Talbot algorithms are competitive with cosine and sine transforms using a lagged convolution digital filtering method and explicit evaluation of the frequency-domain responses at all the required frequencies. They are generally slower, however, than the cosine and sine transforms for which the frequency-domain responses are explicitly computed at several tens of frequencies and the responses at all required frequencies obtained by interpolation. However, the accuracy of such splined cosine and sine transform methods is degraded, potentially making them less accurate than the computationally competitive Euler and Talbot approaches.

ACKNOWLEDGMENTS

We thank K. Key for his open source codes for 1D forward modeling of marine CSEM and B. Barrowes for his open source codes for Anderson's 787-coefficient cosine and sine transforms. We also thank W. Whitt and K. Kuhlman for their help with inverse Laplace transforms. This work was supported by the National Natural Science Foundation of China (nos. 41274077, 41474055, 41504088, and 41572116), the Fundamental Research Funds for the Central Universities (no. CUG130103), and the State Key Laboratory

for GeoMechanics and Deep Underground Engineering, China University of Mining & Technology. J. Li was supported by the China Scholarship Council for one year of study at Memorial University of Newfoundland, for which he is grateful. Finally, the authors also acknowledge R. Mittet and four anonymous reviewers for their constructive comments that helped to improve this paper.

APPENDIX A

THE MAGNETIC FIELD EXCITED BY A VMD ON THE SURFACE OF A STRATIFIED MEDIUM

The formulation considered here for the EM field excited by a VMD and a loop positioned on the surface of the earth employs the $e^{i\omega t}$ time dependence. Based on the theory of Ward and Hohmann (1988), under the quasi-static approximation, the vertical component of the magnetic field excited by a VMD on the surface of an N-layer medium is given in the frequency domain by

$$H_z(r) = \frac{m}{4\pi}\int_0^\infty (1 + r_{\mathrm{TE}})\frac{\lambda^3}{u_0}J_0(\lambda r)\mathrm{d}\lambda, \tag{A-1}$$

and the tangential component of the electric field is given in the below equation:

$$E_\varphi(r) = -\frac{z_0 m}{4\pi}\int_0^\infty (1 + r_{\mathrm{TE}})\frac{\lambda^2}{u_0}J_1(\lambda r)\mathrm{d}\lambda. \tag{A-2}$$

The functional dependency ω comes via parameter u and is given explicitly below. In z_0 and u_0, the subscript 0 denotes the air layer. The m is the magnetic moment of the dipole, r is the horizontal offset between the source and the receiver, λ is equal to $\sqrt{k_x^2 + k_y^2}$, and k_x and k_y are the spatial wavenumber variables of the Fourier transform. The values J_0 and J_1 are the zeroth- and first-order Bessel functions of the first kind. The value r_{TE} is the reflection coefficient, and it is determined as follows:

$$r_{\mathrm{TE}} = \frac{Y_0 - \hat{Y}_1}{Y_0 + \hat{Y}_1}, \tag{A-3}$$

where $\hat{Y}_1$ is the surface admittance of the first layer, and is obtained by the recursion formula:

$$\hat{Y}_1 = Y_1\frac{\hat{Y}_2 + Y_1\tanh(u_1h_1)}{Y_1 + \hat{Y}_2\tanh(u_1h_1)}, \tag{A-4}$$

$$\hat{Y}_n = Y_n\frac{\hat{Y}_{n+1} + Y_n\tanh(u_nh_n)}{Y_n + \hat{Y}_{n+1}\tanh(u_nh_n)}, \tag{A-5}$$

and

$$\hat{Y}_N = Y_N. \tag{A-6}$$

The value Y_n is the intrinsic admittance of the nth layer, and it has the form $Y_n = u_n/z_n$, where $u_n^2 = \lambda^2 - k_n^2$, $k_n^2 = -i\omega\mu_n\sigma_n$, $z_n = i\omega\mu_n$, ω is the angular frequency, μ_n, σ_n, and h_n are the magnetic permeability, conductivity, and thickness for the nth layer. In our research, the magnetic permeability is set to μ_0.

As is well known, air conductivity is extremely low, so the value of u_0 is equal to λ. If N is 1, the reflection coefficient will be $r_{\mathrm{TE}} \approx (\lambda - u_1)/(\lambda + u_1)$ and equation A-1 can be rewritten as follows:

$$H_z(r) = \frac{m}{2\pi}\int_0^\infty \frac{\lambda^3}{\lambda + u_1}J_0(\lambda r)\mathrm{d}\lambda. \tag{A-7}$$

Then, using the Lipschitz and Sommerfeld integrals, the zeroth-order Bessel function can be substituted into equation A-7. Therefore, the following analytic form is obtained as follows:

$$H_z(r) = \frac{m}{2\pi k^2 r^5}[9 - (9 + 9ikr - 4k^2r^2 - ik^3r^3)e^{-ikr}], \tag{A-8}$$

where $k^2 = -i\omega\mu_0\sigma_1$. Based on equation A-8, the formula in the Laplace domain is as follows:

$$H_z(r) = -\frac{m}{2\pi\mu_0\sigma_1 r^5}\left[\frac{9}{s^2} - \left(\frac{9}{s^2} + \frac{9\alpha}{s^{3/2}} + \frac{4\alpha^2}{s} + \frac{\alpha^3}{s^{1/2}}\right)e^{-\alpha s^{1/2}}\right], \tag{A-9}$$

where $\alpha = (\mu_0\sigma_1)^{1/2}r$, and s is the variable in the Laplace domain, which is equal to $i\omega$. Multiplying equation A-9 by s, then using the formulas of inverse Laplace transform, the corresponding impulse response is as follows:

$$\frac{\partial h_z}{\partial t}(r) = \frac{m}{2\pi\mu_0\sigma_1 r^5}\left[9erf(\theta r) - \frac{2\theta r}{\pi^{1/2}}(9 + 6\theta^2r^2 + 4\theta^4r^4)e^{-\theta^2r^2}\right], \tag{A-10}$$

where $erf(\theta r)$ is the error function, $\theta = \sqrt{\mu_0\sigma_1/4t}$, and t is the observation time.

In this study, the Hankel transform integrals in equation A-7 for layered models were computed using the 120-coefficient fast Hankel transform (FHT) of Guptasarma and Singh (1997).

APPENDIX B

THE MAGNETIC FIELD EXCITED BY A RECTANGULAR LOOP ON THE SURFACE OF STRATIFIED MEDIUM

We continue to employ the formulation of the EM field for a VMD established by Ward and Hohmann (1988). Assume that a VMD is located at the origin of Cartesian coordinate system. Using the transform relations between the cylindrical coordinate system and the Cartesian coordinate system, the horizontal components E_x and E_y excited by this VMD at the observing point $(x, y, 0)$ can be deduced from equation A-2:

$$E_x(r) = \frac{z_0 m}{4\pi}\cdot\frac{y}{r}\int_0^\infty (1 + r_{\mathrm{TE}})\frac{\lambda^2}{u_0}J_1(\lambda r)\mathrm{d}\lambda \tag{B-1}$$

and

$$E_y(r) = -\frac{z_0 m}{4\pi}\cdot\frac{x}{r}\int_0^\infty (1+r_{\mathrm{TE}})\frac{\lambda^2}{u_0}J_1(\lambda r)\mathrm{d}\lambda, \qquad \text{(B-2)}$$

where $r=(x^2+y^2)^{1/2}$. In general, a rectangular loop can be regarded as a combination of numerous small VMDs. Assuming that the z-axis is directed vertically downward and the origin is located at the geometric center of this rectangular loop, then $(x', y', 0)$ becomes the coordinates of every small VMD, and r is revised to $[(x'-x)^2+(y'-y)^2]^{1/2}$. By substituting m with $\mathrm{d}m = I\mathrm{d}x'\mathrm{d}y'$ in equations B-1 and B-2, followed by the area integral over the rectangular loop, the electric field excited by this rectangular loop at observing point $(x, y, 0)$ is as follows:

$$E_x(r) = \frac{z_0 I}{4\pi}\int_{-W}^{W}\int_{-L}^{L}\frac{y'-y}{r}\int_0^\infty (1+r_{\mathrm{TE}})\lambda J_1(\lambda r)\mathrm{d}\lambda\mathrm{d}y'\mathrm{d}x' \qquad \text{(B-3)}$$

and

$$E_y(r) = -\frac{z_0 I}{4\pi}\int_{-W}^{W}\int_{-L}^{L}\frac{x'-x}{r}\int_0^\infty (1+r_{\mathrm{TE}})\lambda J_1(\lambda r)\mathrm{d}\lambda\mathrm{d}y'\mathrm{d}x', \qquad \text{(B-4)}$$

where W and L are half sides of the rectangular loop. In the above two equations, λ^2/u_0 is replaced by λ due to the extremely low conductivity of air. Then, using the following relation (Ward and Hohmann, 1988)

$$\frac{\partial J_0(\lambda r)}{\partial y'} = -\lambda\frac{y'-y}{r}J_1(\lambda r), \qquad \text{(B-5)}$$

equation B-3 becomes

$$E_x(r) = -\frac{z_0 I}{4\pi}\int_{-W}^{W}\int_0^\infty (1+r_{\mathrm{TE}})[J_0(\lambda r_L) - J_0(\lambda r_{-L})]\mathrm{d}\lambda\mathrm{d}x', \qquad \text{(B-6)}$$

and equation B-4 can be rewritten as follows:

$$E_y(r) = \frac{z_0 I}{4\pi}\int_{-L}^{L}\int_0^\infty (1+r_{\mathrm{TE}})[J_0(\lambda r_W) - J_0(\lambda r_{-W})]\mathrm{d}\lambda\mathrm{d}y', \qquad \text{(B-7)}$$

where I is the exciting current, and W and L are half sides of the rectangular loop, $r_L=[(x'-x)^2+(L-y)^2]^{1/2}$, $r_{-L}=[(x'-x)^2+(-L-y)^2]^{1/2}$, $r_W=[(W-x)^2+(y'-y)^2]^{1/2}$, and $r_{-W}=[(-W-x)^2+(y'-y)^2]^{1/2}$.

Based on Faraday's law, the magnetic field impulse response can be transformed from the electric field, for example, the vertical component is as follows:

$$\frac{\partial b_z(r)}{\partial t} = F^{-1}\left(\frac{\partial E_x(r)}{\partial y}\right) - F^{-1}\left(\frac{\partial E_y(r)}{\partial x}\right), \qquad \text{(B-8)}$$

where F^{-1} means the inverse Fourier transform. The formula of, for example, $\partial E_x(r_L)/\partial y$ in the frequency domain is as follows:

$$\frac{\partial E_x(r_L)}{\partial y} = -\frac{z_0 I}{4\pi}\frac{L-y}{r_L}\int_{-W}^{W}\int_0^\infty \lambda(1+r_{TE})J_1(\lambda r_L)\mathrm{d}\lambda\mathrm{d}x'. \qquad \text{(B-9)}$$

Formulas for $\partial E_x(r_{-L})/\partial y$, $\partial E_y(r_W)/\partial x$, and $\partial E_y(r_{-W})/\partial x$ are obtained in the same way. To accurately solve these integrals with respect to loop size, for example, B-9, we divide the integral interval $[-W, W]$ into two subintervals, namely $[-W, 0]$ and $[0, W]$, and then use Gauss-Legendre quadrature with 12 points for every subinterval. The Hankel transform integrals were computed using the 140-coefficient FHT of Guptasarma and Singh (1997).

APPENDIX C

INLINE HORIZONTAL COMPONENT OF ELECTRIC FIELD FOR THE MARINE CSEM METHOD

Consider an HED located in the ith layer of an N-layered medium. The frequency-domain inline horizontal electric field excited by this HED in the quasi-static approximation can be written as follows (Key, 2012):

$$E_h(r) = \int_0^\infty \left(\hat{E}_{J_0}J_0(\lambda r) + \hat{E}_{J_1}\frac{J_1(\lambda r)}{r}\right)\mathrm{d}\lambda, \qquad \text{(C-1)}$$

where

$$\hat{E}_{J_0}(\lambda) = -\frac{1}{2\pi\mu\sigma_i}\left(u_i^2\hat{A}_h + \lambda^2\frac{\partial\hat{\Lambda}_z}{\partial z}\right)\lambda, \qquad \text{(C-2)}$$

$$\hat{E}_{J_1}(\lambda) = \frac{1}{2\pi\mu\sigma_i}\left(\hat{A}_h + \frac{\partial\hat{\Lambda}_z}{\partial z}\right)\lambda^2, \qquad \text{(C-3)}$$

$u_i^2 = \lambda^2 - i\omega\mu_0\sigma_i$, ω is the angular frequency, r is the horizontal offset between the source and the receiver location, σ_i is the conductivity of the ith layer, μ is the magnetic permeability in vacuum. For marine CSEM, the source and receiver are positioned in the ith layer, and the horizontal and vertical potentials are as follows:

$$\hat{A}_h = a_i e^{u_i(z-z_{i+1})} + b_i e^{-u_i(z-z_i)} + \frac{\mu}{2u_i}e^{-u_i|z-z_s|}, \qquad \text{(C-4)}$$

and

$$\hat{\Lambda}_z = c_i e^{u_i(z-z_{i+1})} + d_i e^{-u_i(z-z_i)} - \frac{u_i}{\lambda^2}(a_i e^{u_i(z-z_{i+1})} - b_i e^{-u_i(z-z_i)}), \qquad \text{(C-5)}$$

where z_s, z_i, and z are the source depth, the top depth of the ith layer, and the measurement depth, respectively. Detailed expressions for a_i, b_i, c_i, and d_i are given in Key (2009).

The above formulation is based on the $e^{-i\omega t}$ time dependence. Therefore, if we compute the time-domain responses by inverse Laplace transform, the variable s in the Laplace domain will be replaced by $-i\omega$, whereas u_i^2 is still $\lambda^2 + s\mu\sigma_i$. For this scenario, the Hankel transform integrals were computed using the 201-coefficient FHT of Key (2012).

REFERENCES

Abate, J., G. L. Choudhury, and W. Whitt, 1996, On the Laguerre method for numerically inverting Laplace transforms: INFORMS Journal on Computing, **8**, 413–427, doi: 10.1287/ijoc.8.4.413.

Abate, J., G. L. Choudhury, and W. Whitt, 1999, An introduction to numerical transform inversion and its application to probability models, *in* W. K. Grassman, ed., Computational probability: Springer, 257–323.

Abate, J., and P. P. Valkó, 2004, Multi-precision Laplace transform inversion: International Journal for Numerical Methods in Engineering, **60**, 979–993, doi: 10.1002/(ISSN)1097-0207.

Abate, J., and W. Whitt, 1992, The Fourier-series method for inverting transforms of probability distributions: Queueing Systems, **10**, 5–87, doi: 10.1007/BF01158520.

Abate, J., and W. Whitt, 2006, A unified framework for numerically inverting Laplace transforms: INFORMS Journal on Computing, **18**, 408–421, doi: 10.1287/ijoc.1050.0137.

Anderson, W. L., 1983, Fourier cosine and sine transforms using lagged convolutions in double-precision (subprograms DLAGF0/DLAGF1): Technical Report 83-320, U.S. Geological Survey.

Barsukov, P. S., and E. B. Fainberg, 2014, Transient marine electromagnetics in shallow water: A sensitivity and resolution study of the vertical electric field at short ranges: Geophysics, **79**, no. 1, E39–E49, doi: 10.1190/geo2013-0125.1.

Börner, R. U., O. G. Ernst, and K. Spitzer, 2008, Fast 3-D simulation of transient electromagnetic fields by model reduction in the frequency domain using Krylov subspace projection: Geophysical Journal International, **173**, 766–780, doi: 10.1111/gji.2008.173.issue-3.

Connell, D., and K. Key, 2013, A numerical comparison of time and frequency-domain marine electromagnetic methods for hydrocarbon exploration in shallow water: Geophysical Prospecting, **61**, 187–199, doi: 10.1111/gpr.2013.61.issue-1.

Constable, S., 2010, Ten years of marine CSEM for hydrocarbon exploration: Geophysics, **75**, no. 5, 75A67–75A81, doi: 10.1190/1.3483451.

Constable, S., and C. J. Weiss, 2006, Mapping thin resistors and hydrocarbons with marine EM methods: Insights from 1D modeling: Geophysics, **71**, no. 2, G43–G51, doi: 10.1190/1.2187748.

d'Ozouville, N., E. Auken, K. Sorensen, S. Violette, G. d'Marsily, B. Deffontaines, and G. Merlen, 2008, Extensive perched aquifer and structural implications revealed by 3D resistivity mapping in a Galápagos volcano: Earth and Planetary Science Letters, **269**, 518–522, doi: 10.1016/j.epsl.2008.03.011.

Effersø, F., E. Auken, and K. I. Sørensen, 1999, Inversion of band-limited TEM responses: Geophysical Prospecting, **47**, 551–564, doi: 10.1046/j.1365-2478.1999.00135.x.

Everett, M. E., 2009, Transient electromagnetic response of a loop source over a rough geological medium: Geophysical Journal International, **177**, 421–429, doi: 10.1111/gji.2009.177.issue-2.

Everett, M. E., and R. N. Edwards, 1993, Transient marine electromagnetics: The 2.5-D forward problem: Geophysical Journal International, **113**, 545–561, doi: 10.1111/gji.1993.113.issue-3.

Farquharson, C. G., and D. W. Oldenburg, 1993, Inversion of time-domain electromagnetic data for a horizontally layered earth: Geophysical Journal International, **114**, 433–442, doi: 10.1111/gji.1993.114.issue-3.

Flis, M. F., G. A. Newman, and G. W. Hohmann, 1989, Induced-polarization effects in time-domain electromagnetic measurements: Geophysics, **54**, 514–523, doi: 10.1190/1.1442678.

Flores, C., and S. A. Peralta-Ortega, 2009, Induced polarization with in-loop transient electromagnetic soundings: A case study of mineral discrimination at El Arco porphyry copper, Mexico: Journal of Applied Geophysics, **68**, 423–436, doi: 10.1016/j.jappgeo.2009.03.009.

Goldman, M. M., and D. V. Fitterman, 1987, Direct time-domain calculation of the transient response for a rectangular loop over a two-layer medium: Geophysics, **52**, 997–1006, doi: 10.1190/1.1442368.

Gupta, P. K., A. P. Raiche, and F. Sugeng, 1989, Three-dimensional time-domain electromagnetic modelling using a compact finite-element frequency-stepping method: Geophysical Journal International, **96**, 457–468, doi: 10.1111/gji.1989.96.issue-3.

Guptasarma, D., and B. Singh, 1997, New digital linear filters for Hankel J0 and J1 transforms: Geophysical Prospecting, **45**, 745–762, doi: 10.1046/j.1365-2478.1997.500292.x.

Hohmann, G. W., 1983, Three-dimensional EM modeling: Geophysical Surveys, **6**, 27–53, doi: 10.1007/BF01453994.

Jang, H., H. Jang, K. H. Lee, and H. J. Kim, 2013, Step-off, vertical electromagnetic responses of a deep resistivity layer buried in marine sediments: Journal of Geophysics and Engineering, **10**, 025011, doi: 10.1088/1742-2132/10/2/025011.

Kano, P. O., M. Brio, and J. V. Moloney, 2005, Application of Weeks method for the numerical inversion of the Laplace transform to the matrix exponential: Communications in Mathematical Sciences, **3**, 335–372, doi: 10.4310/CMS.2005.v3.n3.a4.

Key, K., 2009, 1D inversion of multicomponent, multifrequency marine CSEM data: Methodology and synthetic studies for resolving thin resistive layers: Geophysics, **74**, no. 2, F9–F20, doi: 10.1190/1.3058434.

Key, K., 2012, Is the fast Hankel transform faster than quadrature? Geophysics, **77**, no. 3, F21–F30, doi: 10.1190/geo2011-0237.1.

Knight, J. H., and A. P. Raiche, 1982, Transient electromagnetic calculations using the Gaver-Stehfest inverse Laplace transform method: Geophysics, **47**, 47–50, doi: 10.1190/1.1441280.

Kuhlman, K. L., 2013, Review of inverse Laplace transform algorithms for Laplace-space numerical approaches: Numerical Algorithms, **63**, 339–355, doi: 10.1007/s11075-012-9625-3.

Li, J. H., Z. Q. Zhu, S. C. Liu, and S. H. Zeng, 2011, 3D numerical simulation for the transient electromagnetic field excited by the central loop based on the vector finite-element method: Journal of Geophysics and Engineering, **8**, 560–567, doi: 10.1088/1742-2132/8/4/008.

Li, Y. G., and S. Constable, 2010, Transient electromagnetic in shallow water: Insights from 1D modeling: Chinese Journal of Geophysics, **53**, 737–742, doi: 10.3969/j.issn.0001-5733.2010.03.029.

Meju, M. A., P. J. Fenning, and T. R. W. Hawkins, 2000, Evaluation of small-loop transient electromagnetic soundings to locate the Sherwood Sandstone aquifer and confining formations at well sites in the Vale of York, England: Journal of Applied Geophysics, **44**, 217–236, doi: 10.1016/S0926-9851(00)00005-7.

Montella, C., R. Michel, and J. P. Diard, 2007, Numerical inversion of Laplace transforms. A useful tool for evaluation of chemical diffusion coefficients in ion-insertion electrodes investigated by PITT: Journal of Electroanalytical Chemistry, **608**, 37–46, doi: 10.1016/j.jelechem.2007.05.011.

Newman, G. A., G. W. Hohmann, and W. L. Anderson, 1986, Transient electromagnetic response of a 3D body in a layered earth: Geophysics, **51**, 1608–1627, doi: 10.1190/1.1442212.

Porsani, J. L., C. A. Bortolozo, E. R. Almeida, E. N. S. Sobrinho, and T. G. D. Santos, 2012, TDEM survey in urban environmental for hydrogeological study at USP campus in São Paulo city, Brazil: Journal of Applied Geophysics, **76**, 102–108, doi: 10.1016/j.jappgeo.2011.10.001.

Raiche, A. P., 1987, Transient electromagnetic field computations for polygonal loops on layered earths: Geophysics, **52**, 785–793, doi: 10.1190/1.1442345.

Raiche, A. P., D. L. B. Jupp, H. Rutter, and K. Vozoff, 1985, The joint use of coincident loop transient electromagnetic and Schlumberger sounding to resolve layered structures: Geophysics, **50**, 1618–1627, doi: 10.1190/1.1441851.

Sasaki, Y., M. J. Yi, J. Choi, and J. S. Son, 2015, Frequency and time domain three-dimensional inversion of electromagnetic data for a grounded-wire source: Journal of Applied Geophysics, **112**, 106–114, doi: 10.1016/j.jappgeo.2014.09.016.

Stehfest, H., 1970, Algorithm 368, numerical inversion of Laplace transforms: Communications of the ACM, **13**, 47–49, doi: 10.1145/361953.361969.

Swidinsky, A., and R. N. Edwards, 2009, The transient electromagnetic response of a resistive sheet: Straightforward but not trivial: Geophysical Journal International, **179**, 1488–1498, doi: 10.1111/gji.2009.179.issue-3.

Swidinsky, A., R. N. Edwards, and M. Jegen, 2013, The marine controlled source electromagnetic response of a steel borehole casing: Applications for the NEPTUNE Canada gas hydrate observatory: Geophysical Prospecting, **61**, 842–856, doi: 10.1111/gpr.2013.61.issue-4.

Talbot, A., 1979, The accurate numerical inversion of Laplace transforms: IMA Journal of Applied Mathematics, **23**, 97–120, doi: 10.1093/imamat/23.1.97.

Valkó, P. P., and J. Abate, 2004, Comparison of sequence accelerators for the Gaver method of numerical Laplace transform inversion: Computers and Mathematics with Applications, **48**, 629–636, doi: 10.1016/j.camwa.2002.10.017.

Ward, S. H., and G. W. Hohmann, 1988, Electromagnetic theory for geophysical applications, *in* M. N. Nabighian, ed., Electromagnetic methods in applied geophysics: Theory: SEG 1, 131–252.

Weeks, W. T., 1966, Numerical inversion of Laplace transforms using Laguerre functions: Journal of the Association for Computing Machinery, **13**, 419–429, doi: 10.1145/321341.321351.

Woods, V. W., 2006, Geophysical report on a fixed-loop and borehole transient EM survey, Grid area C, Red hill property: Avalon Ventures Ltd.

Xue, G. Q., L. J. Gelius, P. A. Sakyi, N. N. Zhou, W. Y. Chen, B. C. Su, H. Li, H. S. Zhong, and Y. P. Su, 2014, Discovery of a hidden BIF deposit in Anhui province, China by integrated geological and geophysical investigations: Ore Geology Reviews, **63**, 470–477, doi: 10.1016/j.oregeorev.2014.05.007.

Yang, D., and D. W. Oldenburg, 2012, Three-dimensional inversion of airborne time-domain electromagnetic data with applications to a porphyry deposit: Geophysics, **77**, no. 2, B23–B34, doi: 10.1190/geo2011-0194.1.